Operation of SOFC Short-Stacks with Simulated Bio-Syngas: Influence of Model Tars Naphthalene and Phenol

Michael Hauser[a], Stephan Herrmann[a,*], Sebastian Fendt[a], Christian Lenser[b], Norbert H. Menzler[b], Hartmut Spliethoff[a]

[a] *Technische Universität München, Institute for Energy Systems, Boltzmannstr 15, 85748 Garching/Germany*
[b] *Forschungszentrum Jülich GmbH, Institute of Energy and Climate Research, IEK-1: Materials Synthesis and Processing, 52425 Jülich/Germany*

Abstract

Operation of solid oxide fuel cells (SOFCs) with bio-syngas from the gasification of biomass is a promising approach to highly efficient and sustainable power generation. At the same time, the coupling is intricate as several biogenic impurities in the bio-syngas have a damaging effect on the SOFC. For this paper the impacts of the impurities naphthalene and phenol on anode-supported solid oxide fuel cells with Ni/YSZ anode integrated in short-stacks were investigated experimentally. The experiments were performed at 700 °C under load with simulated bio-syngas consisting of hydrogen, carbon monoxide, carbon dioxide, methane and water vapour. 2 g/Nm^3 of naphthalene (350 ppm) caused a pronounced voltage drop and an increase in cell temperature. By analysing the anode off-gas and recording of I-V-curves, it could be shown that naphthalene blocked the electrochemical hydrogen oxidation as well as the reforming of methane and the shift reaction of carbon monoxide. Up to 8 g/Nm^3 (190 ppm) phenol, on the other hand, led to carbon depositions and irreversibly damaged the structure of the anode substrate by metal dusting. This form of degradation was not visible in the electrochemical data during operation.

*Corresponding author
Email address: stephan.herrmann@tum.de (Stephan Herrmann)
URL: http://www.es.mw.tum.de (Stephan Herrmann)

Keywords: SOFC, bio-syngas, tar, naphthalene, phenol, short-stack, metal dusting

1. Introduction

The majority of solid oxide fuel cell (SOFC) systems are currently operated directly on natural gas or on fossil hydrogen produced by methane steam reforming [1]. As this creates fossil CO_2 emissions, it is more sustainable to operate the SOFC on bio-syngas instead, which is produced by gasification of solid biomass. The interconnection of gasifier and SOFC is called biomass integrated gasification fuel cell system (B-IGFC). A very high electrical efficiency of 63 $\%_{\mathrm{LHV}}$ can be achieved by such a B-IGFC at a total exergetic efficiency of 55 % for an optimised interconnection, in which the heat of post-combustion of unconverted fuel gas and a part of the waste heat of the SOFC are introduced into the gasifier via heat pipes and a part of the anode exhaust gas is recycled [2].

Bio-syngas mainly consists of hydrogen (H_2), methane (CH_4), carbon monoxide (CO), carbon dioxide (CO_2), water (H_2O) and nitrogen (N_2) [3]. In addition to these main gas components, the raw bio-syngas contains impurities in the form of particles, sulphur, alkali and chlorine compounds and tars [4, 5, 6]. In this context tars are higher hydrocarbons which result from incomplete conversion of complex biogenic macro-molecules in the gasifier. Tars can potentially block catalytic centres for both electrochemical and reforming reactions, inhibit the diffusion of fuel, or lead to mechanical deterioration of the cell [7]. At the same time they can be reformed at the SOFC anode and serve as a fuel.

The successful coupling of gasifier and SOFC with complete removal of all impurities was shown by several authors using different setups [8, 9, 10, 11]. Fischer et al. [12] have operated two F10 short-stacks from Forschungszentrum Jülich at 700 °C with the bio-syngas from an allothermal fluidised-bed gasifier. During the first test with complete gas cleaning (particles, chlorine- and sulphur components, tars and unsaturated hydrocarbons) the stack performance was

stable and there were no carbon deposits or material-related problems. The test on the second short-stack without tar-removal had to be stopped after 5.4 h. The reason for this was that carbon deposits in the form of carbon whiskers had formed inside the stack [13] which blocked the fuel gas flow and increased the pressure drop drastically. Under these deposits metal dusting of the anode support had started at the entrance of all cells, which also affected the nickel meshes for contacting. Metal dusting is a type of corrosion which affects different metals - especially iron and nickel - in gases with high carbon activity [14]. Due to carburisation of nickel and the resulting stress on the cermet matrix, disintegration takes place, resulting in metal dust [15].

The tar concentration in the test by Fischer et al. was approx. $5\,g/Nm^3$, mainly consisting of benzene, toluene, cresol, phenol and naphthalene. As these tars were all present at the same time, it was not possible to determine which components caused the damage to the anode. In order to find this out, tests with individual model tars are necessary. Tests with naphthalene as model tar were conducted by several authors [16, 17, 18, 19].

Papurello et al. [16] tested the influence of naphthalene on Ni/YSZ ASCs at $0.33\,A/cm^2$ and 750 °C: in pure H_2 30 ppm of naphthalene ($0.17\,g/Nm^3$) did not affect the performance of the cell negatively whereas 10 ppm ($0.06\,g/Nm^3$) in syngas drastically decreased the cell potential. Additionally using I-V-curves, the authors stated that naphthalene inhibited both electrochemical and reforming reactions. Naphthalene therefore did not only adsorb on the nickel surface at the active sites for reforming, but also at the TPB where electrochemical oxidation takes place. In the worst case the reduction of available fuel by the shortfall of H_2 from reforming could lead to critical fuel utilisation levels and consequently to nickel oxidation at the anode.

Like Papurello et al., Hauth et al. [17] saw the multiple effects of naphthalene for Ni/GDC anodes when adding $11.6\,g/Nm^3$ of it to either hydrogen or syngas at 900 °C. For the first case the authors reported an increase of the OCV whereas it decreased in the second case. The increase in OCV during H_2 operation cannot be interpreted as a relevantly successful usage of naphthalene:

in OCC usually a minimum number of free TPB exists with which the Nernst voltage can be reached and the Nernst voltage is increased by partial reforming of naphthalene. During operation under load, however, naphthalene poisoning manifested itself for all fuel gas mixtures in an increased over-voltage caused by a reduced amount of free TPB, as discussed by [16]. In addition, during syngas operation Hauth et al. detected an increased concentration of CH_4 in the anode off-gas due to naphthalene poisoning of methane reforming. It is remarkable that naphthalene was able to block CH_4 reforming even at an operation temperature of 900 °C. This phenomenon and a decrease in cell voltage were also observed by Dekker et al. [18] when operating a Ni/GDC ESC at 850 °C using syngas and naphthalene as model tar. They reported analogue effects for phenantrene and pyrene.

All studies with naphthalene have in common that no carbon deposits or structural changes of the cell were reported. In contrast, benzene and toluene can lead to severe carbon deposits at the cell. Using these two model tars in dry H_2 plus N_2, Mermelstein et al. reported carbon deposits and subsequent metal dusting on Ni/YSZ ESC at 775 °C [20].

Previous investigations by the authors of this paper have shown the effects of phenol [21] and naphthalene [19] on anode-supported single-cells with Ni/YSZ anode and Ni/YSZ substrate. Up to $4\,g/Nm^3$ phenol in simulated bio-syngas had no effect on electrochemistry, but caused heavy carbon deposition and metal dusting. $0.4\,g/Nm^3$ of naphthalene, on the other hand, did not cause carbon deposition, but interfered with the electrochemistry as it led to a severe decrease of cell voltage. Impedance measurements have shown that naphthalene first inhibited mass transfer in the anode functional layer and only afterwards, when CH_4 and CO as fuel had been eliminated, did it affect mass transfer through the substrate. The polarisation resistance of the electrochemical oxidation itself increased only to a small extent. Tests with other concentrations of naphthalene showed that the decrease of cell voltage correlated with the accumulated amount of the model tar.

Data in literature on the impact of model tars on SOFCs is mostly based

on single-cell tests. In this paper short-stacks were operated on simulated bio-syngas to which the tars naphthalene and phenol were added separately. Phenol and naphthalene were selected as model tars as these are two of the most frequent tar components in bio-syngas from fluidised-bed gasifiers [22]. The stacks were operated under load at 700 °C. In addition to cell voltage, temperatures and pressure drop, I-V-curves were used to measure the impact of the tars. The composition of the anode off-gas was analysed for the detection of inhibition of fuel conversion reactions. After the tests both stacks were opened to check the state of the cells.

2. Experimental

2.1. Tested Short-Stacks

In this work short-stacks in the F10 design of Forschungszentrum Jülich with two or four cells were used. Details on this stack type can be found in [23]. Inside the stack fuel gas and air flow in counterflow, with both gas streams being supplied from below. The interconnectors and cell frames of the stack consist of Crofer 22 APU, which up to 900 °C forms a top layer of electrically conductive chromium-manganese oxide with a low chromium evaporation rate [24]. The individual metal layers are sealed with glass sealant. In order to further reduce chromium evaporation and poisoning of the cathode, a MnCo1.9Fe0.1O4 (MCF) coating is applied via atmospheric plasma spraying (APS) on all exposed parts of the interconnector on the air side [25]. A fine and a coarse nickel mesh is used for contacting at the anode side, and a contact layer of LaMn0.45Co0.35Cu0.2O3 (LCC10) coating is applied onto the cathode via screen printing.

The cell type in the stacks is variable. The cells in the two short-stacks examined in this work had a 10 x 10 cm^2 Ni/3YSZ substrate from CeramTec (Marktredwitz/Germany) printed with the functional layers (Ni/ 8YSZ anode, 8YSZ electrolyte, GDC barrier layer, LSCF cathode) by Jülich [26]. The electrochemically active area in the stack was determined by the size of the cathode of the cells and was 80 cm^2. The end plates and the middle interconnector plate

had three drill holes with a depth of 40 mm each, into which thermocouples could be inserted. With these the temperature inside the stack - 10 mm from air and gas inlet and in the middle of the cells -could be measured. Wires of Pt welded to the end plates and to each interconnector acted as contact for measurement of all cell voltages. The two stacks were both joined at 850 °C for 120 h at Forschungszentrum Jülich followed by reduction of the anodes and reliability tests. The latter had a duration of 180 h for Stack N and 30 h for Stack P. Afterwards they were shipped to TUM for the tests with simulated bio-syngas.

2.2. Short-Stack Test Rig

Since the short-stacks do not generate enough waste heat, they had to be placed inside a 8 kW_{el} furnace to control their temperature. An adapter plate made of high temperature steel (1.4742) was used for the supply and removal of both fuel and air. Four plates made of high temperature steel (1.4828) with a total weight of 50 kg were used as compression weight for stack and sealing. Rods made of Inconel served as connection between the end plates of the stacks and the electrical load (PLI 2106 from Höcherl & Hackl, Konzell/Germany). There was no device for impedance measurements implemented in the stack test rig; for the discussion of the influence of naphthalene on the impedance the reader is referred to [19]. To control the current and measure the stack voltage, thin silver potential wires were connected to the load in parallel. The load could be operated stand-alone or with a LabView programme which also controlled the fuel gas supply. The single-cell voltages were stored either by a data logger (HOBO UX120-006M, Onset, Bourne/USA) or by the LabView programme via an USB interface (RedLab 1208LS, Meilhaus Electronic, Alling/Germany). The latter had a lower resolution which led to scrawly I-V-curves. For the better representation of the I-V-curves data from this device was therefore fitted with a hyperbolic plus linear term ($U(I) = a/(I + b) + c \cdot I + d$). All wires for the voltage measurement and the thermocouples which measured the temperatures in the stack were sheathed in glass fabric insulation to prevent short circuits.

Besides voltage and current all temperature (stack, oven, pipes, tar container) and differential pressure signals (dp_{fuel} $dp_{\mathrm{fuel,in}}$) were recorded.

A mobile gas mixing station was used for operation of the stacks on simulated bio-syngas. With its mass flow controllers the anode could be supplied with H_2, CH_4, CO, CO_2 and N_2. The purities were 5.0, 2.5, 3.0, 4.5 and 5.0, respectively. Steam was dosed with an HPLC-pump which dosed liquid H_2O into a heated main pipe. Oscillations due to the evaporation of the water led to noise in the recorded cell voltages, see for example period from 12 to 16 h in Fig. 2. The anode could also be purged with forming gas during start-up and failure situations via a separate pipe. The supply of forming gas was controlled by a normally-open solenoid valve so that reducing conditions at the anode were ensured even in the event of a power failure. The air volume flow on the cathode side was regulated manually by a float. All fuel pipes were equipped with trace heating to prevent the condensation of tars.

In order to protect the stack in the best possible way in all situations, further safety aspects were taken into account. First, an overflow valve at the fuel gas inlet ensured that the overpressure there could not exceed a design limit of 100 mbar. The under-voltage protection of the load also ensured that the fuel gas utilisation could not reach critical values after a minimum voltage had been specified. When the emergency stop switch of the test rig was activated, the load automatically switched to OCC (open circuit conditions) and the solenoid valve for forming gas opened. The LabView programme also ensured that the flow of CH_4 and CO were stopped if the steam supply was interrupted to prevent carbon depositions.

After passing through a condenser, some of the fuel gas went into the off-gas analysis and the rest was burnt in an outside flare. The pipe to the flare was heated to prevent condensation or freezing of residual moisture. The anode exhaust gas composition after condensation of the water was measured online using a gas analyser (Sick C700, Waldkirch/Germany). The gases CH_4, CO and CO_2 were measured by non-dispersive infra-red absorption (NDIR). For H_2 a thermal conductivity detector (WLD) was used, and a paramagnetic sensor for

O_2 [27]. The ranges for CH_4, CO, CO_2, H_2 and O_2 were 0-10, 0-70, 0-40, 0-40 and 0-25 vol%, respectively. The nitrogen content resulted from the difference to one hundred percent. If the concentration of a component left the respective measuring range, the excess was output as N_2. The response time of the analysis was in the minute range and the realistic accurancy was approx. 1 %. A zero point calibration was performed before each measurement.

2.3. Tar Dosing and Detection

A tube-shaped container filled with tar was used for the dosage of tar during stack tests. The inner diameter of the tube was 56 mm and its length was 180 mm whereas the distance between gas inlet and gas outlet was 150 mm. A heating sleeve was used for accurate temperature control. The container was placed horizontally in order to achieve the largest possible interface between tar and carrier gas (CO_2). For easy filling or cleaning the container was equipped with Tri-Clamp connections. Two thermocouples measured the temperature of the container wall and in the gas outlet. The latter was used to calculate the saturation vapour pressure, and from this the tar concentration in the fuel gas; see appendix for the applied formulas. When the SOFC was operated with tar-laden syngas, the anode off-gas was led through a separate condenser in order to protect downstream equipment from tar contamination.

The actual presence of tar was checked by the solid phase adsorption (SPA) method proposed by Brage et al. [28]. The gas volume for each measurement was 100 ml which was sampled manually using a syringe. As solid phase for tar adsorption Hypersep 100 mg Nh2 columns from ThermoScientific, Rockwood/USA were used. The captured tars could be eluted afterwards with a solvent, here dichloromethane (DCM SupraSolv, Merck, Darmstadt/Germany) was used. The mixture of solvent and tars was collected in 2 ml glass vials. 1 μl of the mixture was injected to the column (19091J-413, Agilent, Santa Clara/ USA) of a gas chromatograph (7890 A from Agilent) which allowed the quantitative analysis of the tar content by integrating the signal of the flame ionisation detector. The short-stack test rig was equipped with three ports for SPA mea-

surements: one after the tar dosing, one upstream and one downstream of the stack. Sampling in the wet anode gas streams was inaccurate since steam condensed in the syringe. Sampling in the dry carrier gas after the tar dosing led to blockage of the needle of the syringe due to the high tar concentration. The SPA method was therefore only used to check the presence of the respective model tar in the fuel inlet and outlet gas and not its amount.

2.4. Procedure of the Tests

After installing the stacks inside the furnace on the adapter plate, they were heated to 700 °C at 4 K/min (furnace set temperature 708 °C). At the same time, 0.5 Nl/ min/cell forming gas were flowing through the fuel gas side to prevent the anode from re-oxidising. The air side flow was 2 Nl/min/cell for the entire duration of the tests from the start of heating. After a stationary temperature was reached a basic characterisation was performed in the form of several I-V-curves with pure hydrogen (1.125 Nl/min/cell H_2), a H_2/H_2O mixture (1.1 Nl/min/cell H_2 and 0.275 Nl/ min/cell = 0.221 mg/min/cell H_2O) and a H_2/N_2 mixture (0.5 Nl/min/cell H_2, 0.61 Nl/min/cell N_2). The rate of current increase was 20 A/min. The basic characterisation was followed by the actual test programmes. The sequence of the test phases and the applied concentrations of naphthalene and phenol are shown in table 1. The volume flow of simulated bio-syngas was 1 Nl/min/cell, and except for Syn_0 at Stack N the applied current was 27 A (current density 0.34 A/cm^2). For the dosing of tars 67 ml/min of the overall CO_2 flow were led through the heated tar container which was either filled with naphthalene or phenol.

3. Results and Discussion

The results of measured cell voltages and I-V-curves, temperatures, pressures, off-gas composition, and the preliminary post-test analysis are shown and discussed in the following.

Table 1: Sequence of the test phases for the short-stack tests. Gas flows during syngas in Nl/min/cell: 0.5 H_2O, 0.25 H_2, 0.1 CO, 0.1 CO_2. 0.05 CH_4; 2 air at cathode. Standard current 27 A.

Reading point	**Start, h**	**Duration, h**	**T_{Tar}, °C**
Stack N			
Initial I-V-curves	-	-	-
Syn_0[§]	0	19	-
Syn	19	1	-
Syn + 2 g/Nm^3 Naph	20	29	81
Syn (recovery)	49	26	-
Forming gas	75	66	-
Syn	141	6	-
Relaunch[*]	1027	52	-
Stack P			
Initial I-V-curves	-	-	-
Syn	0	64	-
Syn + 2 g/Nm^3 Phe	64	24	74
Syn + 4 g/Nm^3 Phe	88	24	87
Syn + 8 g/Nm^3 Phe	104	24	101

[§] 40 A

[*] different mixtures of H_2, N_2 and H_2O

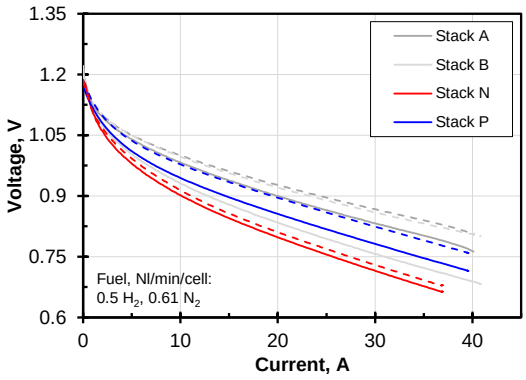

Figure 1: Initial I-V-curves at 0.5 Nl/min/cell H_2 and 0.61 Nl/min/cell N_2 of Stack N and P compared to previously tested stacks. Solid line lower layer (Cell 1), dashed line upper layer (Cell# $\geq$ 2). $T_{\text{stack}} = 700\,^{\circ}\text{C}$. Due to high noise data from Stack P was fitted with a hyperbolic plus linear term for better visibility.

3.1. Initial Characterisation

For both stacks a basic characterisation was performed in the form of several I-V-curves at 700 °C with different reference gas mixtures. Using the curves with 0.5 Nl/min/ cell H_2 and 0.61 Nl/min/cell N_2 as fuel, the stacks could be compared with each other and with previously tested stacks [12] regarding their performance, see figure 1. It can be seen that the performance of Stack N and P was lower but still in accordance with the other stacks. The F10 stacks lose some of their performance each time they are removed from a test stand. In addition, the lowest cell always has a lower cell voltage, which is probably due to the lower temperature caused by heat dissipation through the adapter plate. Since the preheating of the cathode air was optimised before the test on Stack N, its two cells showed minor voltage-deviation from each other in contrast to the other stacks.

3.2. Influence of Naphthalene

Figure 2 shows the time response of the stack voltage from the start of operation of the stack with syngas. There occurred a clear decrease of the voltage within the first 19 h, which can be evaluated as running-in behaviour.

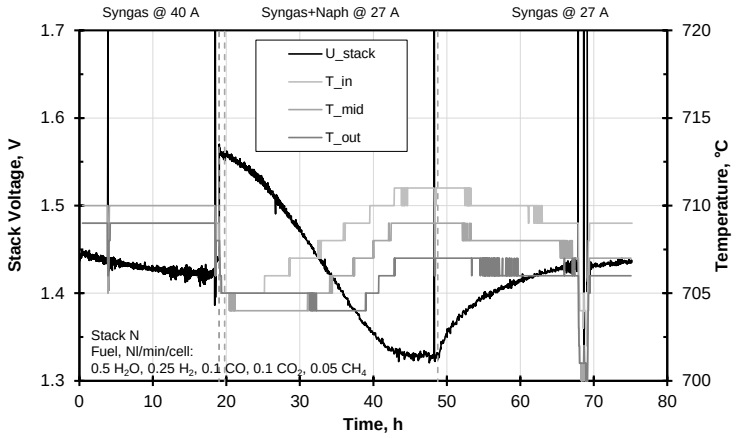

Figure 2: Course of stack voltage and temperatures of the upper cell (inlet, middle, outlet). Syngas as main gas, naphthalene concentration 2 g/Nm^3.

At the end of this running-in process the current was lowered from 40 to 27 A so that the current density (0.34 A/cm^2) was the same as in the previous single-cell measurements [21, 19]. At the same time the slightly larger cell area contacted in the short-stack – 80 instead of 72 cm^2 – led to a higher fuel gas utilisation than in the single-cell tests – 34 % instead of 30 %.

After approximately one hour of operation at syngas and 27 A, 2 g/Nm^3 of naphthalene (350 ppm) were added to the fuel gas. The temperature of the tar container was 81 °C. Complete reforming of the added naphthalene would theoretically have resulted in additional 0.004 Nl/ min/cell H_2 and 0.005 Nl/min/cell CO_2. After a delay of approx. 1 h the voltage dropped steadily, and after 25 hours reached a plateau which was for both cells approx. 110 mV below the voltage last measured with pure syngas. This corresponded to the observations from the previous single-cell tests whereas the rate and absolute value of voltage decrease was lower and the transition to the plateau was smoother. This was probably due to the different tar dosing devices and the longer piping at the short-stack test rig. Overall, the behaviour of the stack was in accordance with the observations of Dekker et al. [18] or Hauth et al. [17] who saw a distinct decrease of performance when adding naphthalene to the fuel gas.

The presence of naphthalene in the fuel gas was regularly tested using SPA samples. Naphthalene was found in all samples upstream of the stack. In the first sample, which was taken 3.5 h after the start of dosing, a lower amount of naphthalene was measured compared to later samples. In the last sample, which was taken 1.5 h after switching back to pure syngas, a small amount of naphthalene was still present in the fuel gas. Both findings indicate that minimal amounts of naphthalene had condensed somewhere in the fuel supply pipes. Naphthalene was also present in the SPA samples of the anode exhaust gas but the amount was small so that the signal of the flame ionisation detector could not be integrated by the software of the gas chromatograph. This means that only a fraction of the supplied naphthalene left the stack unconverted and the balance was adsorbed and slowly reformed.

As in the single-cell tests the voltage drop was accompanied by an increase in temperature. The grey lines in Fig. 2 show the signals of the three thermocouples at the upper cell. The trends of the thermocouples in the lower cell layer behaved parallel to each other, which together with the parallel cell voltages indicated a uniform effect on both cells. The temperature initially increased at the inlet and only with a delay at the middle and the outlet of the cell, which was interpreted as a progressing naphthalene front which inhibited endothermic reforming of methane. This was also confirmed by an increasing amount of non-converted methane in the anode off-gas. The trends of the gas analysis will be discussed later. The pressure drop across the stack fluctuated between 4 and 10 mbar with no observable trend. This was an indication that the flow in the layers had not changed during naphthalene dosing. In contrast to the experiments with phenol, no carbon deposits were to be expected, which would have increased the pressure drop in the stack.

After 29 hours of naphthalene dosage the switch back to pure syngas was carried out, which resulted in the recovery of voltage. After 26 h on syngas – interrupted by a phase with H_2/N_2 as fuel gas for an I-V-curve from hour 67 to 70 – the gas supply was switched to forming gas. The voltage on syngas by then (t = 75 h) was still slowly increasing and had reached 93 % of its original value.

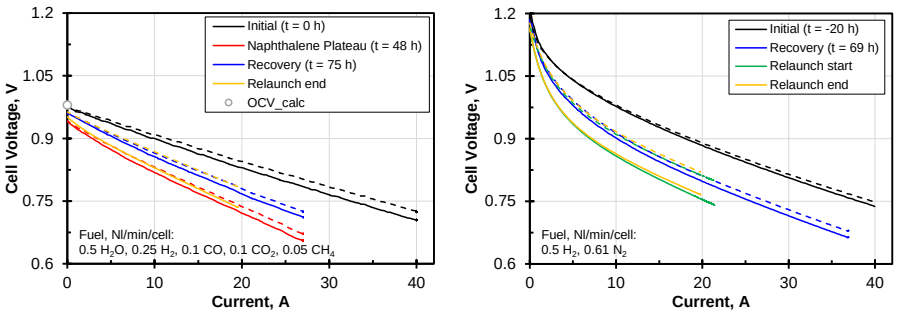

Figure 3: Left: I-V-curves of Stack N on syngas at indicated instants. Right: I-V-curves on H_2/N_2 mixture at indicated instants. Solid lines represent voltage of lower cell. $T_{\text{stack}} = 700\,^{\circ}\text{C}$. Noisy data were fitted with a hyperbolic plus linear term for better visibility.

Again similar behaviour was observed by Dekker et al. [18] who saw that the cell performance recovered when naphthalene was removed from the fuel gas.

Figure 3 left shows the I-V-curves that were recorded on syngas during the test. Compared to the state in the plateau (red curves), the performance had clearly recovered up to the switching to forming gas (blue curves). However, the performance was still far from its original state (black curves); the ASR was increased and the OCV decreased. The comparison of the I-V-curves for syngas and H_2/N_2 in figure 3 shows that the influence of naphthalene poisoning on the OCV (open circuit voltage) was only present in syngas. There are two influences which explain the reduced OCV in syngas: first, the H_2 partial pressure was reduced by unconverted CH_4 and CO and second, less additional H_2 from the conversion of CH_4 and CO was available. Both had an effect on the reactant term in the Nernst equation, resulting in lower OCV. Under load both gas compositions had an increased ASR due to naphthalene poisoning. This again shows that naphthalene did not only block reforming reactions but also directly inhibited electrochemical oxidation of hydrogen or fuel gas diffusion to the TPB, as observed by Papurello et al. [16]. Due to a high voltage drop in the current collectors, it was not possible to set a sufficiently high current during the I-V-curves to make the mass transport limitation through the anode substrate visible. Together with the ASR, this maximum current density would have

provided further data for the interpretation of the poisoning.

After the first part of the test ($t < 75\,\mathrm{h}$) the stack was "parked" for 66 h with a forming gas flow at the fuel gas side and without drawing current. It was noticed that the OCV did not increase further in this phase. Two hypotheses could explain this behaviour. First, the recovery at OCC was not visible because enough triple phase boundaries (TPB) were unpoisoned to deliver the open cell potential. This means that experiments on the influence of naphthalene should always be carried out under load and not at OCC. Second, naphthalene could probably only be removed from anode and substrate by reforming, which would have required water vapour. When resuming the operation with syngas under load (27 A) after the 66 hours, the stack voltage was at the same level as before the forming gas phase, which suggests that no further regeneration had taken place by flushing with forming gas. The stack was cooled down afterwards.

In order to investigate the influence of the fuel gas composition on recovery, the stack was relaunched. The stack had lost performance due to removal and reinstallation and the air preheater was defective during this second run. The stack was operated at 0.5 Nl/min/cell H_2 and 0.5 Nl/min/cell H_2O at the fuel gas side to force the reforming of naphthalene at the anode, intermitted by phases on H_2/Nm and syngas for I-V-curves. When switching back to syngas, however, 3 vol% CH_4 were still present in the exhaust gas, which was interpreted as a clear sign of persistent poisoning. As can be seen from the respective I-V-curves in figure 3, the performance could not be further increased. All I-V-curves on syngas and on H_2/N_2 recorded in the second run were nearly superimposed. Consequently, the stack could not be regenerated by advantageous gas compositions at 700 °C.

In addition to voltage, temperature and pressure drop, the dry exhaust gas composition (CH_4, CO, CO_2, H_2, O_2, balance N_2) was also measured during the stack tests. The value of O_2 was always below 0.1 vol% and therefore was not evaluated further. The qualitative values of the exhaust gas analysis could

be converted into actual volume flows of components. Via a carbon balance

$$\dot{V}_{\mathrm{C,in}} = \dot{V}_{\mathrm{CH_4}} + \dot{V}_{\mathrm{CO}} + \dot{V}_{\mathrm{CO_2}} \tag{1}$$

the volume flows for CO, CO_2 and CH_4 in the outlet could be calculated from their volume proportions. Here ideal gas was assumed, so volume flow corresponded to flow of matter. The values for $\dot{V}_{\mathrm{CH_4}}$, $\dot{V}_{\mathrm{CO}}$, $\dot{V}_{\mathrm{CO_2}}$ were 0.1, 0.2 and 0.2 Nl/min, respectively. Using the example of CH_4:

$$\dot{V}_{\mathrm{CH_4,out}} = \dot{V}_{\mathrm{C,in}} \frac{y_{\mathrm{CH_4}}}{y_{\mathrm{CH_4}} + y_{\mathrm{CO}} + y_{\mathrm{CO_2}}}. \tag{2}$$

From this the total dry volume flow at the outlet

$$\dot{V}_{\mathrm{dry,out}} = \frac{1}{y_{\mathrm{CH_4}} + y_{\mathrm{CO}} + y_{\mathrm{CO_2}}} \dot{V}_{\mathrm{C,in}} \tag{3}$$

could be determined. Since apart from CO, CO_2 and CH_4 only H_2 was present in the flue gas, the H_2 volume flow could be calculated with the total dry volume flow:

$$\dot{V}_{\mathrm{H_2,out}} = \dot{V}_{\mathrm{dry,out}} - \dot{V}_{\mathrm{C,in}}. \tag{4}$$

The results of the dry gas volume flow calculations at the stack outlet are shown in figure 4. For comparison, the curves of the cell voltages (U_1 lower cell and U_2 upper cell) were plotted in grey in the same diagram. The vertical coloured lines indicate the intervals in which the CH_4- or H_2-concentration was outside of the detection limit of the respective sensor, i.e. when $CH_4 > 10\,\mathrm{vol\%}$ or $H_2 > 40\,\mathrm{vol\%}$. As can be seen for CH_4, the addition of the excess N_2 resulted in slight discontinuities in the curves. Fortunately only either H_2 or CH_4 was at its limit in accordance with the measuring ranges. According to the calculation of the volume flow, more CH_4 left the stack at the end of the naphthalene dosing than was fed to it. The overestimation of 20 % (0.12 instead of 0.1 Nl/min) was due to reading errors in gas dosing and analysis.

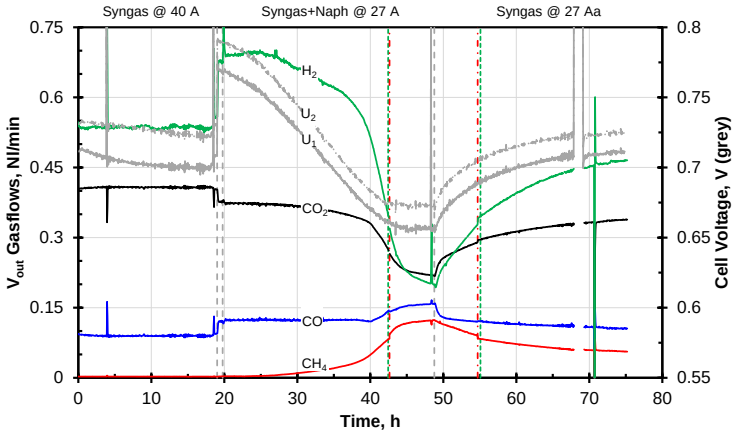

Figure 4: Flow rate of main gas components CO, CO_2, CH_4 and H_2 in the anode exhaust gas during measurement at Stack N. U_1 voltage of lower cell and U_2 voltage of upper cell. T_{stack} = 700 °C.

Initially, no methane was measured in the exhaust gas, which corresponds to the reaction equilibrium for the adjusted syngas composition at 700 °C. However, the increasing proportion of CH_4 in the exhaust gas confirms that the presence of naphthalene blocked the conversion of CH_4 at the anode. Even at the end of syngas operation after the naphthalene phase the poisoning was still pronounced, as can be clearly seen from the increased CH_4 content, analogous to the non-recovered stack voltage. It can also be seen that the CO_2 volume flow decreased significantly in line with decreasing CO and CH_4 conversion when naphthalene poisoning progressed. Since the omission of both reactions led to less H_2 at the anode and the H_2 utilisation had to increase to maintain the current level, the H_2 concentration in the exhaust gas decreased. The CO conversion was very constant initially and it is noticeable that, in contrast to CH_4, the CO flow quickly returned to its original level after the switchover to pure syngas. The reaction kinetics of the endothermic reforming of CH_4 at 700 °C might be slower than the exothermic WGS of CO. This would mean that compared to CH_4 CO would require less non-poisoned cell area to be converted. The fact that CO is formed during the reforming of CH_4 and CO can be used directly

by the SOFC under certain conditions [29, 30] leads to a complex relationship that cannot be clarified on the basis of the collected data alone.

After evaluating the impedance data of the single-cell tests with naphthalene [19], it was assumed that the presence of the tar led directly to the inhibition of fuel diffusion inside the anode functional layer and of the reaction at the TPB. The impairment of reforming activity was observed in the EIS at a later stage. This is now also evident in the stack exhaust gas: the volume flows of CO, CO_2 and H_2 were approximately constant during the first five hours of naphthalene dosing while the voltages of the cells had already dropped by approx. 25 mV. Even the absolute value of CH_4 only rose imperceptibly during this period, but the beginning of its subsequently exponential increase in the exhaust gas can be guessed. During this initial phase naphthalene blocked an increasing number of active centres for electrochemical reactions at the anode so cell voltages dropped while gas conversion across the cell was still nearly constant.

The omission of CH_4 and CO as fuel led to an increase of fuel utilisation (FU): in normal operation it was 34 %; without CH_4 54 %; without CH_4 and CO 75 %, which then represented the hydrogen utilisation. The last H_2 volume flow determined during naphthalene dosing was 0.2 Nl/min, corresponding to an FU_{H_2} of 60 %. For a hydrogen utilisation of 75 % the H_2 volume flow would have had to decrease to 0.125 Nl/min. So reforming and WGS were not completely inhibited at the time of shutdown, which was also indicated by the fact that the gas analysis values were not yet stationary. The further omission of CO and CH_4 might not have led to a further voltage decrease from a certain point in time: It is possible that then it was no longer the amount of available fuel that was limiting for the cell potential but the diffusion to the anode and the rate of the electrochemical reaction at the TPB.

After the end of the measurement, the stack was opened at Forschungszentrum Jülich. Similar to what all single-cell tests with naphthalene had shown [31] there were no macroscopically visible carbon depositions inside the stack. The structure of the cells seemed unaltered; however, a detailed investigation on possible microscopic changes is pending.

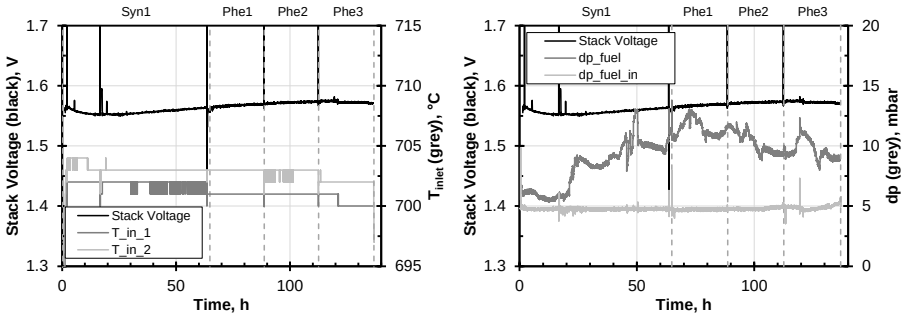

Figure 5: Left: Trends of stack voltage and inlet temperature of lower cell ($T_{\mathrm{in},1}$) and upper cell ($T_{\mathrm{in},2}$) of Stack P. Right: Pressure drop on fuel gas side (p_{fuel}) and overpressure at fuel inlet ($p_{\mathrm{fuel,in}}$) of Stack P.

3.3. Influence of Phenol

After initial I-V-curves Stack P was operated on pure Syngas at 0.34 A/cm^2 for 64 h. Then 2, 4 and 8 g/Nm^3 of phenol (475, 950, 1900 ppm) were added to the syngas for 24 h each. With complete reforming these phenol amounts would have resulted in additional 0.007, 0.014 and 0.028 Nl/min/cell H_2, respectively. The temperatures of the phenol-filled tar container necessary to achieve the desired tar concentrations were 74, 87 and 101 °C, respectively. In contrast to the single-cell tests [21] the phenol phases were conducted without interruption, only the temperature of the tar container was increased. The tar content was regularly checked using the SPA method. Phenol was detected in all samples from the fuel inlet gas and the measured amount doubled for each phenol phase. In the fuel outlet gas no phenol was detected in any sample.

Figure 5 shows the stack voltage during the test. It was subject to a drift of approximately 25 mV which was caused by the bottom cell whereas the voltage of the upper cell was constant. The stack voltage first fell for approx. 20 h after the start of Syn1 and then rose above the original level until Phe3. The reason for this upward drift might have been the shorter reliability tests compared to Stack N. The noise in the voltage signal was due to steady oscillation of the water dosage. During Phe3 a discontinuity occurred at t = 120 h which ended the rise. Apart from this discontinuity, which may be attributed to the known

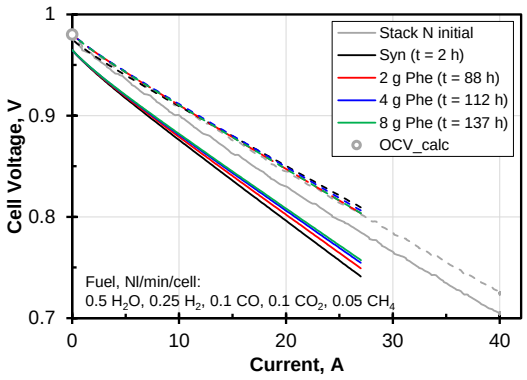

Figure 6: I-V-curves of Stack P on syngas plus 0, 2, 4 and 8 g/Nm^3 of phenol together with data from Stack N. $T_{\mathrm{stack}} = 700\,^{\circ}\mathrm{C}$. Data for Stack P was fitted with a hyperbolic plus linear term for better visibility.

dusting effects of phenol on the substrate [21, 32], the stack voltage did not respond to the presence of tar in the simulated bio-syngas. The shape of the I-V-curves recorded during pure syngas and at every concentration of phenol was similar but followed the upwards trends of the cell voltage under load, see Fig. 6. This shows that as in the single-cell experiments electrochemistry was not affected by phenol within the duration of this test.

Neither did the temperatures in the stack - in figure 5 the fuel gas inlet temperatures in both layers are shown - react to phenol but fell during the experiment analogously to the increasing stack voltage. The pressure drop across the stack dp_{fuel} changed more during Syn1 than during the phenol phases. The overpressure at the inlet $dp_{\mathrm{fuel,in}}$ was constant to a large extent; only starting from the discontinuity at approx. 120 h during Phe3 did a slow increase become apparent. On the basis of the single-cell experiments [21] it was to be expected that the pressure drop would increase due to thermally cracked phenol and metal dusting. Potentially the exposure time was not long enough for these phenomena to occur. On the other hand, the shape of gas flow in the stack is very different compared to the ceramic housing in the single-cell experiments. The materials used - Crofer and nickel instead of ceramic, gold and nickel - might

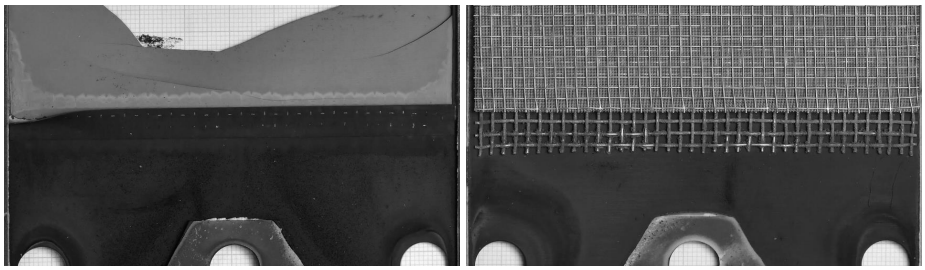

Figure 7: Photos of one layer of Stack P after the tests with phenol. Left: surface of the anode substrate. Right: nickel meshes for contacting.

also have had different influences on the decomposition of phenol upstream of the cells. Since water droplets had formed in the pipes leading to the differential pressure sensors during the measurement, the signals might have been falsified and an increase of pressure drop - if it had actually occurred - might not have been recorded.

Possible alterations of the anode exhaust gas composition could be monitored by the gas analysis. Besides minor drifts the composition was constant during the test. The analysis was not accurate enough to establish a balance with which the amount of carbon deposited in the stack (see Fig. 7) could have been determined.

After the end of the measurement the stack was opened at Forschungszentrum Jülich. Macroscopically visible metal dusting similar to the single-cell tests with phenol as model tar [32] occurred on both cells. The substrate on the fuel gas inlet of both cells was discoloured along the entire width of the cell; see the band of brighter grey along the cell in figure 7 left. In addition, carbon deposits were found on the nickel nets, see figure 7 right. In contrast to the previous short-stack test on tarry real bio-syngas [12], the amount of deposits was small and therefore did not inhibit the gas flow through the stack. It seems that the real bio-syngas contained tar components with a higher potential for carbon deposits. In addition, loose carbon particles were found in the fuel gas manifold, which suggests that phenol was partly cracked upstream of the cells

as in the single-cell experiments. A detailed examination of the stack and the cells using microscopy and Raman spectroscopy has not been carried out so far. It would be interesting to find out if the morphology of the carbon deposits was different compared to the previous tests on real tars [12], as it was similarly observed by Lorente et al. [7]: using temperature programmed oxidation they observed that pure toluene led to more stable carbon deposits compared to a mixture of real tars [7].

4. Conclusion

In addition to previous single-cell experiments with naphthalene and phenol as model tar components, tests were carried out on two two-level short-stacks at 700 °C for investigations under application-oriented conditions. The results of the single-cell tests could be reproduced and broadened with the short-stack tests.

In accordance with literature naphthalene led to a strong decrease in voltage, an increase in cell temperature and to the inhibition of the conversion of methane and carbon monoxide. The latter could be monitored by the analysis of the anode off-gas and led to a higher consumption of hydrogen. All effects partly reversed when the supply of naphthalene was stopped. No full recovery of the stack voltage and gas conversion could be established, even when applying hydrogen plus steam as fuel gas. The I-V-curves recorded confirmed that naphthalene in syngas operation reduced both the OCV and the operating voltage under load. With H_2/N_2 as fuel gas an over-potential could also be found with persistent naphthalene poisoning, but the OCV was unaffected. This shows that naphthalene not only inhibited reforming and CO shift, reducing H_2 partial pressure, but also blocked H_2 reactions and mass transfer to TPB.

Phenol had no detectable influence on cell voltage, temperature, pressure drop and the composition of the anode off-gas. Only post-mortem analysis revealed carbon deposits at the cells and the nickel nets and starting metal dusting. The extent of these changes was not yet large enough to interfere with

the operation of the stack; but in the long run a decrease of performance is to be expected.

The cells in the stacks were anode-supported with a Ni/YSZ anode. The tests showed that this cell type is not suitable for operation with tar-containing bio-syngas under the operating conditions applied, especially at a moderate temperature of 700 °C. Future improvement of the cells must aim at accelerated reforming of naphthalene and other hydrocarbons. In addition, the formation of carbon deposits must be prevented as these act as a trigger for metal dusting, which negatively affects both the cells and other materials inside the stack.

5. Acknowledgements

The investigations presented here are supported by Deutsche Forschungsgemeinschaft (DFG) which is gratefully acknowledged (SP *367/5-1*). Moreover, we would like to thank Ute de Haart and Dr. Quingping Fang for carrying out the reduction of the stacks at Forschungszentrum Jülich and Dr. Carole Babelot for the photographs of the opened stacks.

References

[1] E4tech, Fuel cell industry review 2019, Tech. rep., E4tech (2019).
URL `http://www.FuelCellIndustryReview.com`

[2] S. Herrmann, Innovative thermodynamic cycles for renewable energy supply, Ph.D. thesis, Technische Universität München (2018).

[3] M. Kaltschmitt, H. Hartmann, H. Hofbauer, Energie aus Biomasse, 3rd Edition, Springer Vieweg, Berlin Heidelberg, 2016.

[4] F. Kirnbauer, V. Wilk, H. Kitzler, S. Kern, H. Hofbauer, The positive effects of bed material coating on tar reduction in a dual fluidized bed gasifier, Fuel 95 (2012) 553–562.

[5] M. Mayerhofer, P. Mitsakis, X. Meng, W. de Jong, H. Spliethoff, M. Gaderer, Influence of pressure, temperature and steam on tar and gas in allothermal fluidized bed gasification, Fuel 99 (2012) 204–209.

[6] T. S. Doyle, Z. Dehouche, P. V. Aravind, M. Liu, S. Stankovic, Investigating the impact and reaction pathway of toluene on a SOFC running on syngas, International Journal of Hydrogen Energy 39 (23) (2014) 12083–12091.

[7] E. Lorente, M. Millan, N. P. Brandon, Use of gasification syngas in SOFC: Impact of real tar on anode materials, International Journal of Hydrogen Energy 37 (8) (2012) 7271–7278.

[8] P. Hofmann, A. Schweiger, L. Fryda, K. D. Panopoulos, U. Hohenwarter, J. D. Bentzen, J. P. Ouweltjes, J. Ahrenfeldt, U. Henriksen, E. Kakaras, High temperature electrolyte-supported Ni-GDC/YSZ/LSM SOFC operation on two-stage Viking gasifier product gas, Journal of power sources 173 (1) (2007) 357–366.

[9] F. P. Nagel, S. Ghosh, C. Pitta, T. J. Schildhauer, S. Biollaz, Biomass integrated gasification fuel cell systems–concept development and experimental results, Biomass and bioenergy 35 (1) (2011) 354–362.

[10] N. Dekker, B. Van der Drift, L. Rabou, H. Van Wees, B. Rietveld, Operation of a Staxera SOFC stack fuelled with cleaned gas from a gasifier, in: 8th European SOFC & SOE Forum 2008, 2008.

[11] R. Ø. Gadsbøll, J. Thomsen, C. Bang-Møller, J. Ahrenfeldt, U. B. Henriksen, Solid oxide fuel cells powered by biomass gasification for high efficiency power generation, Energy 131 (2017) 198–206.

[12] F. Fischer, M. Hauser, M. Hauck, S. Herrmann, S. Fendt, H. Jeong, C. Lenser, N. H. Menzler, H. Spliethoff, Effect of internal hydrocarbon reforming during coupled operation of a biomass gasifier with hot gas cleaning and SOFC stacks, Energy Science & Engineering (2019).

[13] H. Jeong, M. Hauser, F. Fischer, M. Hauck, S. Lobe, R. Peters, C. Lenser, N. H. Menzler, O. Guillon, Utilization of bio-syngas in solid oxide fuel cell stacks: Effect of hydrocarbon reforming, Journal of The Electrochemical Society 166 (2) (2019) F137–F143.

[14] S. Forseth, P. Kofstad, Metal dusting phenomenon during carburization of FeNiCr-alloys at 850–1000°, Materials and Corrosion 46 (4) (1995) 201–206.

[15] J. Zhang, P. Munroe, D. J. Young, Microprocesses in nickel accompanying metal dusting, Acta Materialia 56 (1) (2008) 68–77.

[16] D. Papurello, A. Lanzini, P. Leone, M. Santarelli, The effect of heavy tars (toluene and naphthalene) on the electrochemical performance of an anode-supported SOFC running on bio-syngas, Renewable Energy 99 (2016) 747–753.

[17] M. Hauth, W. Lerch, K. König, J. Karl, Impact of naphthalene on the performance of SOFCs during operation with synthetic wood gas, Journal of Power Sources 196 (17) (2011) 7144–7151.

[18] N. J. J. Dekker, J. P. Ouweltjes, A. Van der Drift, G. Rietveld, Efficient conversion of biogas in electricity and heat by a solid oxide fuel cell, in: Proceedings of the 15th European biomass conference & exhibition, Berlin, Germany, 2007.

[19] M. Hauser, S. Herrmann, M. Hauck, S. Fendt, H. Jeong, C. Lenser, N. H. Menzler, H. Spliethoff, Effects of naphthalene on the performance of Ni/YSZ anode-supported SOFCs, ECS Transactions 91 (1) (2019) 697–706.

[20] J. Mermelstein, M. Millan, N. P. Brandon, The impact of carbon formation on Ni–YSZ anodes from biomass gasification model tars operating in dry conditions, Chemical Engineering Science 64 (3) (2009) 492–500.

[21] M. Geis, S. Herrmann, S. Fendt, H. Jeong, C. Lenser, N. H. Menzler, H. Spliethoff, Coupling SOFCs to biomass gasification – The influence of

phenol on cell degradation in simulated bio-syngas. Part I: Electrochemical analysis, International Journal of Hydrogen Energy 43 (45) (2018) 20417–20427.

[22] M. Mayerhofer, Teerentstehung und Teerminderung bei allothermer Wirbelschichtvergasung, Ph.D. thesis, Technische Universität München (2014).

[23] Q. Fang, L. Blum, R. Peters, M. Peksen, P. Batfalsky, D. Stolten, SOFC stack performance under high fuel utilization, International journal of hydrogen energy 40 (2) (2015) 1128–1136.

[24] Crofer 22 apu data sheet, download 08.11.2019 (2010).
URL https://www.vdm-metals.com/fileadmin/user_upload/Downloads/Data_Sheets/Datenblatt_VDM_Crofer_22_APU.pdf

[25] N. Grünwald, D. Sebold, Y. J. Sohn, N. H. Menzler, R. Vaßen, Self-healing atmospheric plasma sprayed Mn1. 0Co1. 9Fe0. 1o4 protective interconnector coatings for solid oxide fuel cells, Journal of Power Sources 363 (2017) 185–192.

[26] J. Joos, M. Ender, I. Rotscholl, N. H. Menzler, E. Ivers-Tiffée, Quantification of double-layer Ni/YSZ fuel cell anodes from focused ion beam tomography data, Journal of power sources 246 (2014) 819–830.

[27] L. Briesemeister, Flugstromvergasung hydrothermal karbonisierter Biomasse mit Luft, Ph.D. thesis, Technische Universität München (2018).

[28] C. Brage, Q. Yu, G. Chen, K. Sjöström, Use of amino phase adsorbent for biomass tar sampling and separation, Fuel 76 (2) (1997) 137–142.

[29] M. Homel, T. M. Gür, J. H. Koh, A. V. Virkar, Carbon monoxide-fueled solid oxide fuel cell, Journal of Power Sources 195 (19) (2010) 6367–6372.

[30] M. Riegraf, M. P. Hoerlein, R. Costa, G. Schiller, K. A. Friedrich, Sulfur poisoning of electrochemical reformate conversion on nickel/gadolinium-doped ceria electrodes, ACS Catalysis 7 (11) (2017) 7760–7771.

[31] H. Jeong, Coupling a solid oxide fuel cell with a biomass gasifier: Degradation mechanisms and alternative anode materials, Ph.D. thesis, RWTH Aachen (2019).

[32] H. Jeong, M. Geis, C. Lenser, S. Lobe, S. Herrmann, S. Fendt, N. H. Menzler, O. Guillon, Coupling SOFCs to biomass gasification – The influence of phenol on cell degradation in simulated bio-syngas. Part II: Post-test analysis, International Journal of Hydrogen Energy 43 (45) (2018) 20911–20920.

[33] K. Ruzicka, M. Fulem, V. Ruzicka, Recommended vapor pressure of solid naphthalene, Journal of Chemical & Engineering Data 50 (6) (2005) 1956–1970.

[34] R. Perry, D. Green, Perry's Chemical Engineers' Handbook, 8th Edition, McGraw-Hill Education, New York, 2008.

[35] Dortmund data bank: Vapor pressure of naphthalene, download 18.02.2020 (2019).
URL `http://www.ddbst.com/en/EED/PCP/VAP_C123.php`

[36] ECN, Tar dew point calculation, `http://www.thersites.nl/completemodel.aspx`.

Appendix: Saturation Pressure of Phenol and Naphthalene

In order to obtain a desired concentration of tar in the fuel gas, a constituent equation is necessary with which the saturation vapour pressure p_{sat} can be calculated as a function of temperature. If the saturation vapour pressure is known, the concentration of tar in the fuel gas in g/Nm^3 can be calculated:

$$c = \frac{p_{\mathrm{sat}}}{p} \cdot \frac{\dot{V}_{\mathrm{cg}}}{\dot{V}_{\mathrm{Anode}}} \cdot \frac{MW_{\mathrm{Tar}}}{V_{\mathrm{mol,ig}}} \cdot 1000 \ \frac{\mathrm{l}}{\mathrm{Nm}^3}. \tag{.1}$$

Here $\dot{V}_{\mathrm{cg}}$ is the volume flow of carrier gas through the tar container and $\dot{V}_{\mathrm{Anode}}$ is the total volume flow at the anode. It is assumed that the gas behaves

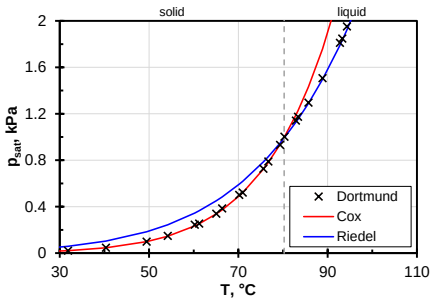

Figure .8: Trend of saturation pressure of naphthalene calculated with Cox and Riedel equation. Experimental reference values are found in [35].

ideally and reaches saturation in the tank (partial pressure = saturation pressure), given the residence is high enough. $V_{\mathrm{mol,ig}}$ is the volume of 1 mole of an ideal gas.

For the calculation of the saturation vapour pressure, a distinction must be made between whether the tar is present in a solid or liquid state, i.e. whether an equilibrium is established between the solid and gas phases or between the liquid and gas phases. For the first case the Cox equation can be used for naphthalene

$$\ln\frac{p_{\mathrm{sat}}}{p_{\mathrm{ref}}} = (1 - \frac{T_{\mathrm{ref}}/K}{T/K})\exp(\sum_{i=0}^{n} a_i (T/K)^i) \tag{.2}$$

with parameters $a_0 = 3.272310$, $a_1 = -2.663498 \cdot 10^{-2}$, $a_2 = -2.929123 \cdot 10^{-9}$, $T_{\mathrm{ref}} = 353.37K$, $p_{\mathrm{ref}} = 993.5Pa$ [33]. For temperatures above 80.3 °C, i.e. for the gas/liquid equilibrium, the Riedel equation can be used

$$\ln\, p_{\mathrm{sat}} = b_0 + \frac{b_1}{T} + b_2 \cdot \ln\, T + b_3 T^{b_4}. \tag{.3}$$

For naphthalene the coefficients are $b_{0,\mathrm{N}} = 61.447$, $b_{1,\mathrm{N}} = -8109$, $b_{2,\mathrm{N}} = -5.5571$, $b_{3,\mathrm{N}} = 2.08 \cdot 10^{-18}$ and $b_{4,\mathrm{N}} = 6$ [34].

As can be seen in figure .8 the two equations in the respective validity ranges very well represent the experimentally measured saturation vapour pressure of naphthalene [35]. In order to determine the necessary container temperature

for a desired tar concentration, the correct equation can be selected with the aid of the required saturation vapour pressure.

For phenol the saturation pressure was calculated with the Riedel equation. Between 314 (melting point) and 694 K the coefficients are $b_{0,\mathrm{P}} = 95.44$, $b_{1,\mathrm{P}} = -10113$, $b_{2,\mathrm{P}} = -10.09$, $b_{3,\mathrm{P}} = 6.76\ \mathrm{e}^{-18}$ and $b_{4,\mathrm{P}} = 6$ [34]. For temperatures below 314 K other coefficients for a solid/gas equilibrium must be applied. No reference data could be found for phenol so it is assumed that the coefficients from [34] are of the same quality as for naphthalene.

This website http://www.thersites.nl/completemodel.aspx [36] offers an online calculation of the dew point temperatures for gases containing defined amounts of tars.